Wave propagation in a dynamic system of soft granular materials

Shusaku Harada*
Department of Mechanical Systems Engineering, University of the Ryukyus, 1 Senbaru, Nishihara-cho, Okinawa 903-0213, Japan

Shu Takagi and Yoichiro Matsumoto
Department of Mechanical Engineering, The University of Tokyo, 7-3-1 Hongo, Bunkyo-ku, Tokyo 113-8656, Japan
(Received 28 November 2002; published 30 June 2003)

The wave propagation in a dynamic system of soft elastic granules is investigated theoretically and numerically. The perturbation theory for simple fluids is applied to the elastic granular system in order to relate the elastic properties of individual particles with the ''thermodynamic'' quantities of the system. The properties of a piston-driven shock are derived from the obtained thermodynamic relations and the Rankine-Hugoniot relations. The discrete particle simulation of a piston-driven shock wave in a granular system is performed by the discrete element method. From theoretical and numerical results, the effect of the elastic properties of a particle on shock properties is shown quantitatively. Owing to the finite duration of the interparticle contact, the compressibility factor of the elastic granular system decreases in comparison with that of the hard-sphere system. In addition, the relation between the internal energy and the granular temperature changes due to the energy preserved with the elastic deformation of the particle. Consequently, the shock properties in soft particles are considerably different from those in the hard-sphere system. We also show the theoretical prediction of the speed of sound in soft particles and discuss the effect of the elasticity on an acoustic wave.

DOI: 10.1103/PhysRevE.67.061305 PACS number(s): 45.70.−n

I. INTRODUCTION

The wave propagation in granular materials can be widely seen in industrial processes or natural phenomena, and is the fundamental subject in the fields of fluid mechanics, strength of material, soil mechanics, and physics. It plays an important role in energy transport in granular materials. The typical example is the fluidization of granules under vibration, which is called the vibrofluidized bed. In the vibrofluidized bed, the energy input by a vibrating wall is transmitted within the granular bed by the compression wave and is converted to the local ''thermal'' energy [1–4]. Such a wave is caused by both the kinetic and the collisional energy transfer, therefore it shows a different behavior in static and dynamic granular systems.

An elastic wave in a static granular system at maximum (or closely maximum) concentration is an important phenomenon in the fields of soil mechanics and geophysics. In such a system, the wave propagates through the contact network of the constituent particles. A lot of studies on the elastic wave propagating in the static granular layer have been carried out theoretically [5,6], experimentally [7], and numerically [8,9]. Some of these studies have suggested that the wave speed depends on the elastic properties of the particle and the confining pressure, and it shows the power-law dependence on the pressure [6].

On the other hand, in a dynamic granular system in which the particles move around, the wave propagates by the contact between particles, which occurs dynamically, and also by particle motion. In order to analyze such a dynamic system, the granular kinetic theory has been developed on the basis of the kinetic theory of molecules. By the kinetic approach, the propagation of the acoustic wave [10,11] and the shock wave [12,13] in granular materials have been studied accounting for the energy loss during the particle collision.

In these kinetic analyses, the particle has been treated as a rigid particle (hard sphere). Accordingly, the wave speed goes to infinity at maximum volumetric concentration since the collision between particles occurs instantaneously. As indicated in the studies on a static system, the wave speed does not go to infinity at maximum concentration because the particle collision costs a finite time. Similarly, the collision time may affect the wave speed in a dynamic system at dense concentration such that the collision occurs frequently.

In this study, we examine the wave propagation in a dynamic system of soft granular materials. Our interest is mainly focused on the effect of the elastic properties of particles on the propagating wave. In order to make the role of the elasticity clear, we treat the conservative system of granular materials, which consists of perfectly smooth and elastic particles. As is well known, the wave propagating in actual granular materials decays owing to the energy dissipation during particle collision. In the case of piston-driven shock, the particles near the piston solidify with the decrease of the kinetic energy by nonconservative collisions and, consequently, a stationary layer of particles is formed on the piston [12,13]. However, it is expected that the constitutive relations derived in this study can be the basis of those in nonconservative systems. In addition, the results shown here can be a rough estimation of wave properties in inelastic particles. This is because the effect of the particle elasticity on the propagating wave is, as will be mentioned below, due to the finite contact time of particles. There is not much difference between the contact time of elastic particles and that of inelastic (but nearly elastic) particles, provided that they have the same elastic properties.

Besides, we focus on the wave at dilute-medium volumet-

*Electronic address: harada@tec.u-ryukyu.ac.jp

ric concentration less than 0.5 and do not deal with the denser system. This is because the phase transition due to crystallization occurs even in rigid particles at dense concentration [14,15], and it is difficult to analyze the system by means of the statistical approach.

In this paper, the constitutive relations for the thermodynamic variables in soft granules are derived by the perturbation approach analogous to that for molecular dynamics. In the theoretical analysis, a dimensionless parameter, which represents the influence of the ''softness'' of the particle on the macroscopic properties, is introduced. Subsequently, the properties of a one-dimensional shock wave formed in granules are derived from the obtained thermodynamic relations. The theoretical results are compared with the corresponding results of the discrete numerical simulation. From both results, the effect of the softness of particles on the shock properties is discussed quantitatively. Furthermore, in the last part of the paper, the speed of sound is calculated from the thermodynamic relations of soft granular materials and is compared with that in a hard-sphere system derived from the kinetic theory.

II. NUMERICAL METHODS

In order to examine the detailed properties of the wave propagates in granular materials and to confirm the results of the theoretical analysis described below, a three-dimensional numerical simulation of granular motions has been performed. The discrete element method (DEM) proposed by Cundall and Strack [16] is used for the calculation of the interaction between particles.

DEM is the method for the Lagrangian simulation of particle motion, and it has been used for the analyses of static and dynamic granular systems [17,18]. In DEM, an interparticle (and also a particle-wall) contact is modeled by using a spring, and the energy dissipation during the contact is expressed by a dashpot and a slider. As described above, the particles are assumed to be perfectly elastic and smooth spheres in the present work. Therefore, the dissipation effect is not considered here and the contact force is treated as a potential force with a cutoff. Consequently, it is identical with that of molecular dynamics simulation.

In the present study, the Hertzian contact force is applied to the contact force model. The elastic contact force between spherical particles is given by [19]

$$F=\sqrt{\frac{16}{9\pi^2}\frac{R_1R_2}{(K_1+K_2)^2(R_1+R_2)}}\delta^{3/2}, \tag{1}$$

where subscripts 1 and 2 indicate the particles in contact, R_1 and R_2 denote the particle radii, and K_1 and K_2 are the elastic constants [$K=(1-\sigma_p^2)/\pi E_p$, E_p is Young's modulus and σ_p is Poisson's ratio). δ is the distance between two spheres and if we set r as the distance between their centers, then $\delta=R_1+R_2-r$. When two spheres are identical ($R_1=R_2=R$, $K_1=K_2=K$), Eq. (1) becomes

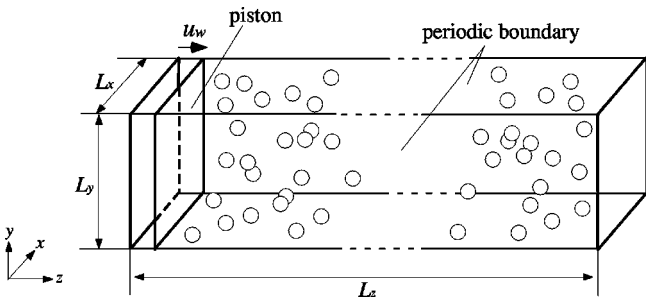

FIG. 1. Schematic diagram of the calculation system.

$$F=\frac{\sqrt{2R}E_p}{3(1-\sigma_p^2)}(2R-r)^{3/2}. \tag{2}$$

In the DEM simulation, the particle motion is calculated individually by integrating the equation of motion. If the particle overlaps with other particles (i.e., $r<2R$), the contact force given by Eq. (2) is exerted on them in the direction of their relative position vector. In the case of the contact between a particle and a solid wall, the normal contact force is calculated by Eq. (1) with $R_2=\infty$ on the assumption that the elastic properties of the wall are the same as those of the particle.

In this work, the motion of particles is calculated from the equation of motion without gravity. The numerical scheme and the algorithm are the same as those given by Tsuji *et al.* [18]. The particle density ρ_p and the radius R are set to be constant, and $\rho_p=2500$ kg/m^3 and $R=0.5$ mm, respectively. The softness of the particle is given by changing the Young's modulus, while the Poisson's ratio is unchanged. In the DEM simulation, the time step Δt has to be set according to the elastic properties so that the energy of the particle is conserved during collision. We decided Δt by preliminary calculations and set $\Delta t=1\times10^{-5}$ s for $E_p=1\times10^6$ Pa and 1×10^7 Pa, and $\Delta t=2\times10^{-6}$ s for $E_p=1\times10^9$ Pa.

Figure 1 is the schematic diagram of the calculation domain and the coordinate system. The boundary conditions in x and y directions are applied to the periodic boundary. In the z direction, one boundary is placed on a piston (solid wall) which moves with a constant speed u_w, and the other is a fixed wall. The length of the domain in the z direction is constant ($L_z=1000R$) and the others (L_x, L_y) are changed according to the condition of the particle concentration.

As for the numerical condition, the initial particle concentration, the initial particle velocity and the piston speed are given, while any statistical information is not given at the boundaries in the same way as Woo and Greber [20]. Initially, 90 000 particles are randomly arranged in the calculation domain and the Maxwell-Boltzmann distribution is applied to their thermal velocity. The calculation is kept on running during the period that the generated wave reflects several times between the piston and the opposite wall. This period corresponds to about 0.1~0.2 s in the simulation. The thermodynamic variables in a cross section are calculated from the numerical results of the number density and the fluctuation velocity of the particle in the finite volume $L_x\times L_y\times\Delta L_z$, where $\Delta L_z=4R$.

III. THEORETICAL APPROACH

The thermodynamic perturbation method is used in order to relate the elastic properties of individual particles to the thermodynamic properties of granular materials. This method is commonly used for the derivation of the equation of state for simple fluids [21–23]. In the present study, the method proposed by Mansoori and Canfield [23] is employed.

An elastic contact force can be treated as a potential force if the energy dissipation during collision is neglected. From Eq. (2), the potential corresponding to the elastic contact force between spherical particles $\phi(r)$ is defined as follows:

$$\phi(r)=\begin{cases}\Gamma\left(1-\dfrac{r}{2R}\right)^{5/2}, & r\leqslant 2R\\ 0, & r>2R,\end{cases} \tag{3}$$

where $\Gamma=16R^3E_p/15(1-\sigma_p^2)$. The total potential energy in the system Φ is assumed to be given by the sum of a two-body interaction potential $\phi(r)$ as

$$\Phi=\sum_{i>j=1}^{N}\phi(r_{ij}), \tag{4}$$

where N is the total number of particles in the system and r_{ij} is the distance between particles i and j. The total potential energy Φ is expressed by the sum of the potential of the reference system Φ_0 and the perturbation Φ' as

$$\Phi=\Phi_0+\Phi'. \tag{5}$$

If the system obeys the classical statistical theory, the Helmholtz free energy A is calculated from the configuration integral. The difference in the Helmholtz free energy between the original and the reference system $A-A_0$ is expressed as follows:

$$A-A_0=-kT\ln\left(\frac{1}{Z_0}\int_V\cdots\int\exp[-\Phi/kT]dr_1\cdots dr_N\right), \tag{6}$$

where Z_0 $(=\int_V\cdots\int\exp[-\Phi_0/kT]dr_1\cdots dr_N)$ is the configurational integral of the reference system, V is the occupied volume, and T is the temperature. k is the Boltzmann constant in the statistical mechanics, however if we consider T as the granular temperature $(=\overline{c^2}/3\ \mathrm{m^2/s^2}$, c is the fluctuation velocity of the particle), k is interpreted simply as a particle mass m_p.

Substituting Eq. (5) into Eq. (6), the approximation of $A-A_0$ is obtained as follows [21,23]:

$$\begin{aligned}A-A_0&=-kT\ln\left(\frac{1}{Z_0}\int_V\cdots\int\exp[-\Phi'/kT]\right.\\&\quad\left.\times\exp[-\Phi_0/kT]dr_1\cdots dr_N\right)\\&\sim\langle\Phi'\rangle_0,\end{aligned} \tag{7}$$

where $\langle\cdots\rangle_0$ indicates the average over the configurations in the reference system, i.e., $\langle a\rangle_0=\int_V\cdots\int a\exp[-\Phi_0/kT]dr_1\cdots dr_N/Z_0$. The relation similar to Eq. (7) is also derived from the Gibbs-Bogoliubov inequality [24] and is given by

$$A-A_0\leqslant\langle\Phi'\rangle_0. \tag{8}$$

It is found from Eq. (8) that the Helmholtz free energy A does not exceed the sum of the Helmholtz free energy in the reference system and the average of the perturbed potential $A_0+\langle\Phi'\rangle_0$.

$\langle\Phi'\rangle_0$ can be expressed by using the perturbed pair potential ϕ' $(=\phi-\phi_0$, ϕ_0: the pair potential of the reference system) and the pair distribution function in the reference system $g_0^{(2)}(r)$ as follows:

$$\langle\Phi'\rangle_0=2\pi nN\int_0^\infty\phi'(r)g_0^{(2)}(r)r^2dr, \tag{9}$$

where $n=N/V$ is the number density. Choosing a hard-sphere potential with diameter d as the reference potential (if $r<d$, $\phi_0=\infty$, otherwise $\phi_0=0$), $g_0^{(2)}(r)$ is zero for $r<d$ and, consequently, Eq. (9) is expressed as

$$\langle\Phi'\rangle_0=2\pi nN\Gamma d^3\int_1^{1/\zeta}(1-\zeta x)^{5/2}g_0^{(2)}(x)x^2dx, \tag{10}$$

where $x=r/d$ and $\zeta=d/2R$.

$A-A_0$ in Eq. (7), and also in inequality (8), can be replaced with $A^e-A_0^e$, where A^e corresponds to the difference of the free energy from the no-potential system, i.e., $A^e=A-A_{ideal}$ (A_{ideal} is the Helmholtz free energy of an ideal gas). Substituting Eq. (10) into Eq. (7), the free energy A^e is approximately given by

$$A^e=A_0^e+2\pi nN\Gamma d^3\int_1^{1/\zeta}(1-\zeta x)^{5/2}g_0^{(2)}(x)x^2dx. \tag{11}$$

Using $A^{e*}=A^e/NkT$ and $T^*=kT/\Gamma(=m_pT/\Gamma$ in the granular system), we obtain a dimensionless form of Eq. (11) as

$$A^{e*}=A_0^{e*}+\frac{12\nu_h}{T^*}\int_1^{1/\zeta}(1-\zeta x)^{5/2}g_0^{(2)}(x)x^2dx, \tag{12}$$

where $\nu_h=n\pi d^3/6=4n\pi(R\zeta)^3/3$ is the volumetric fraction of the hard sphere. The pair distribution function of the reference system (hard-sphere system), $g_0^{(2)}(x)$, is obtained from the integral equation of the distribution function. With the Percus-Yevick approximation [25], $g_0^{(2)}(x)$ is approximately given by the following polynomial with respect to x [26,27]:

$$\begin{aligned}g^{(2)}(x)=\frac{1}{(1-\nu_h)^4}\{&(1+2\nu_h)^2-6\nu_h(1+0.5\nu_h)^2x\\&+0.5\nu_h(1+2\nu_h)^2x^3\}.\end{aligned} \tag{13}$$

Equation (13) is valid only near $x=1$, however $1/\zeta$ in Eq. (12) is almost close to unity because the elastic potential ϕ in an actual system is generally close to the hard-sphere potential ϕ_0.

A^{e*} shown in Eq. (12) is related to the compressibility factor $z=pV/NkT$ as follows:

$$z=1+n\frac{\partial A^{e*}}{\partial n}. \tag{14}$$

The compressibility factor in the hard-sphere system z_0 is given by the function of the volumetric fraction ν_h from the analytical solution of the Percus-Yevick equation [26,27]. It is known that the arithmetic average of the solution of the virial and the Ornstein-Zernike relations is a good approximation of the compressibility in the hard-sphere system [28] and is given by

$$z_0=\frac{1+\nu_h+\nu_h^2-1.5\nu_h^3}{(1-\nu_h)^3}. \tag{15}$$

Substituting Eq. (15) into Eq. (14) and integrating Eq. (14), A^{e*} is obtained as a function of n^* $(=8nR^3)$, T^*, and ζ:

$$A^{e*}=\frac{1}{2}\ln(1-\nu_h)+\frac{3}{1-\nu_h}+\frac{3}{4(1-\nu_h)^2}-\frac{15}{4}+S(n^*,T^*,\zeta), \tag{16}$$

where

$$S(n^*,T^*,\zeta)=\frac{12\nu_h}{T^*}\int_1^{1/\zeta}(1-\zeta x)^{5/2}g_0^{(2)}(x)x^2dx$$

and $\nu_h=\pi n^*\zeta^3/6$. Based on the Gibbs-Bogoliubov inequality (8), the minimum of the right-hand side (RHS) of Eq. (16) with respect to ζ can be considered to be the approximate value of A^{e*}.

According to thermodynamics, the equation of state and the equation for internal energy are expressed by using the Helmholtz free energy A^{e*} and are given by

$$p=\frac{NkT}{V}z=nkT\left(1+n^*\frac{\partial A^{e*}}{\partial n^*}\right), \tag{17}$$

$$\frac{E}{Nk}=-T^2\frac{\partial}{\partial T}\left(\frac{A}{NkT}\right)=T\left(\frac{3}{2}-T^*\frac{\partial A^{e*}}{\partial T^*}\right), \tag{18}$$

respectively. If we consider T as the granular temperature, Eqs. (17) and (18) are expressed as follows:

$$p=\rho_p\nu Tz,\quad z=\left(1+n^*\frac{\partial A^{e*}}{\partial n^*}\right), \tag{19}$$

$$e=\psi T,\quad \psi=\left(\frac{3}{2}-T^*\frac{\partial A^{e*}}{\partial T^*}\right), \tag{20}$$

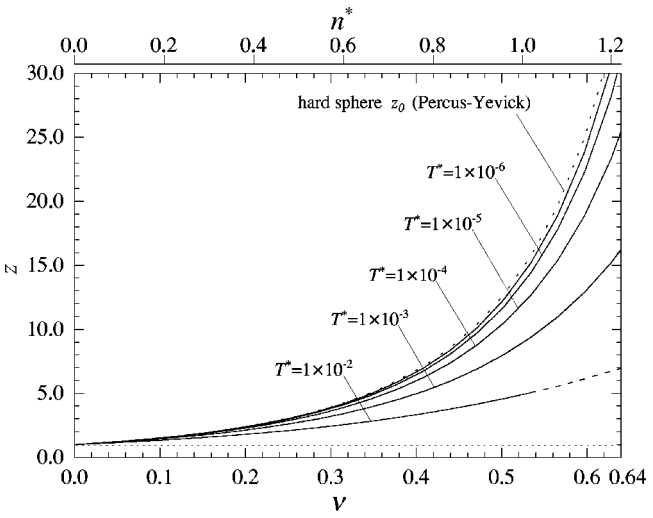

FIG. 2. Compressibility factor z versus ν and n^* for various dimensionless temperatures T^*.

where $\nu=\pi n^*/6$ is the volumetric solid fraction in the original system and $e=E/Nm_p$ is the internal energy per unit mass. Equation (19) is interpreted as the equation of state of the elastic granular system. The term $n^*\partial A^{e*}/\partial n^*$ corresponds to the virial term. On the other hand, Eq. (20) is the relation between the internal energy and the granular temperature. The term $-T^*\partial A^{e*}/\partial T^*$ is related to the preserved energy due to the elastic deformation, as explained below.

In order to obtain z and ψ from Eqs. (19) and (20), some numerical techniques are needed. The right-hand side of Eq. (16) is calculated numerically for given n^*, T^*, and ζ by using Simpson's integral rule, and then ζ_m, which minimizes the right-hand side of Eq. (16), is found numerically. Substituting ζ_m into Eq. (16), we obtain the approximate value of A^{e*} for given n^* and T^*. Applying the same procedure to the calculation for $n^*\pm\Delta n^*$ and $T^*\pm\Delta T^*$, the derivatives $n^*\partial A^{e*}/\partial n^*$ and $T^*\partial A^{e*}/\partial T^*$ are also obtained numerically. In this study, we set $\Delta T^*=0.01T^*$ and $\Delta n^*=0.01n^*$, respectively.

IV. RESULTS AND DISCUSSION

A. Pressure and internal energy of granules

By Eqs. (19) and (20), the elastic properties of individual particles can be related to the macroscopic thermodynamic properties of granular materials. Figures 2 and 3 show z and ψ, which are obtained from Eqs. (19) and (20), respectively, plotted against density for various dimensionless temperature $T^*=m_pT/\Gamma$. As mentioned above, $g_0^{(2)}(x)$ given by Eq. (13), which is used for the calculation of Eq. (16), is valid only near $x=1$ and deviates from the exact solution as being apart from $x=1$. The numerical solution of the Percus-Yevick equation have been shown by Throop and Bearman [29]. In Figs. 2 and 3, the results that the difference between Eq. (13) and the solution by Throop *et al.* is less than 1% of the absolute value are shown by the solid lines, and the other less-accuracy data are shown by the broken lines.

It is shown in Fig. 2 that, when ν (or n^*) is small, the compressibility factor z approaches 1, which corresponds to

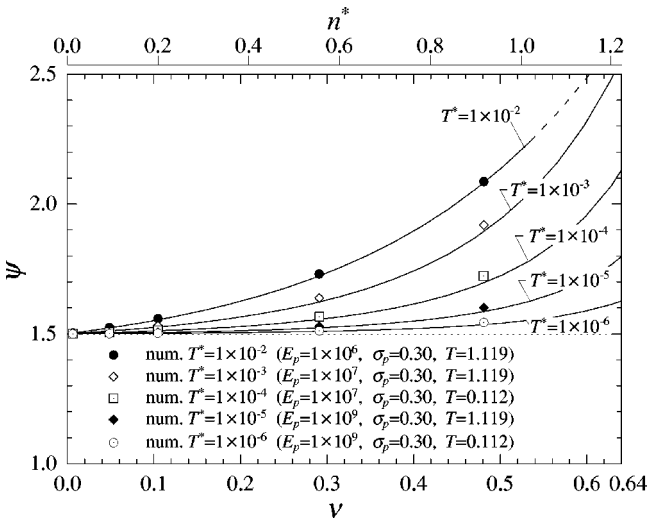

FIG. 3. ψ versus ν and n^* for various dimensionless temperatures T^* (E_p is Young's modulus in Pa, σ_p is Poisson's ratio, and T is the granular temperature in m^2/s^2).

that of an ideal gas. z is increased with the increase in ν and, if T^* is significantly small, it is close to that of the hard-sphere system z_0 given by Eq. (15). On the other hand, as T^* is increased, which means that the particle is heavier and softer for a given fluctuation velocity, z becomes small and deviates from the hard-sphere system. As is expected, if the density and the granular temperature are constant, the pressure is smaller in the softer particles.

Figure 3 shows that ψ is increased with the increase in T^*. This implies that the total energy is divided into the kinetic (thermal) energy and the elastic energy due to the deformation of the particle. When T^* is small, ψ is close to the value for the monatomic gas $\psi=3/2$. This is because the interaction between particles occurs instantaneously and, consequently, most of the energy turns into the kinetic energy. On the other hand, as T^* increases, ψ increases because the contact time is significantly large and some part of the energy is always preserved as the elastic energy. The quantitative discussions on the contact time are given below.

ψ can be also estimated numerically by the DEM simulation. It is obtained from the following procedure. The particles are arranged randomly in a fixed volume so as not to overlap each other, and the Maxwell-Boltzmann velocity distribution is applied to them in the form of initial velocity c. After the simulation is started, the total kinetic energy of the system decreases from the initial energy and then it becomes constant. ψ is given by the ratio of the initial energy per unit mass $\overline{c^2}/2$ to the granular temperature T in a steady state. The results obtained from the DEM simulation are also shown in Fig. 3 by symbols. It is found that ψ obtained theoretically agree well with the corresponding results by the DEM simulation.

The dimensionless temperature T^* ($=m_pT/\Gamma$), which is derived in the process of the perturbation analysis, can be understood more clearly by considering the relation to the contact time. Using the mean fluctuation velocity $\overline{c}$, the particle radius R, the particle density ρ_p, and the elastic constants, T^* can be rewritten as follows:

$$T^*=\frac{5}{32}\pi^2\rho_p\frac{1-\sigma_p^2}{E_p}(\overline{c})^2, \tag{21}$$

where the relation for the Maxwell-Boltzmann velocity $\overline{c^2}=3\pi(\overline{c})^2/8$ is used.

The mean duration of the Hertzian contact is obtained from the differential equation of the relative distance between the colliding particles. The duration of contact with the impact velocity v_c is given by [19]

$$t_c=2.943\frac{\delta_m}{\overline{v_c}}, \tag{22}$$

where $\delta_m=[15m_p\overline{v_c}^2(1-\sigma_p^2)/8\sqrt{2R}E_p]^{2/5}$ is the approach distance at the maximum compression. The coefficient on the RHS of Eq. (22) is resultant from the Γ functions (see Ref. [19]).

The mean impact velocity $\overline{v_c}$ is given by the mean relative velocity $\sqrt{2}\overline{c}$ multiplied by a factor due to the impact angle $2/3$ ($=\int_0^{\pi/2}\cos\theta\sin 2\theta d\theta$), where θ is the angle between the relative velocity vector and the relative position vector of the colliding particles. Substituting $\overline{v_c}=2\sqrt{2}\overline{c}/3$ into Eq. (22), t_c is expressed as follows:

$$t_c=5.913R\left(\rho_p\frac{1-\sigma_p^2}{E_p}\right)^{2/5}(\overline{c})^{-1/5}. \tag{23}$$

On the other hand, the mean free time t_λ, which is the mean time between collisions of a particle, can be roughly estimated as follows. On the assumption that the effect of the particle deformation is significantly small, i.e., the mean free time is the same as that of hard sphere, t_λ is obtained from the mean free time in the dilute system $t_{\lambda 0}$ and the radial distribution function of the hard-sphere system, $g(\nu)[=g_0^{(2)}(1)]$ as follows [30]:

$$t_\lambda=\frac{t_{\lambda 0}}{g(\nu)}. \tag{24}$$

$t_{\lambda 0}$ is obtained by dividing the mean free path $\lambda_0=R/3\sqrt{2}\nu$ by $\overline{c}$. Substituting this relation into Eq. (24), we obtain

$$t_\lambda=\frac{R}{3\sqrt{2}\nu\overline{c}g(\nu)}. \tag{25}$$

Consequently, the ratio of the mean contact time t_c to the mean free time t_λ is calculated from Eqs. (23) and (25) as

$$t_r=\frac{t_c}{t_\lambda}=25.08\nu g(\nu)\left(\rho_p\frac{1-\sigma_p^2}{E_p}\right)^{2/5}(\overline{c})^{4/5}=21.09\nu g(\nu)T^{*2/5}. \tag{26}$$

From Eq. (26), it is found that T^* is simply the function of ν and t_r. If ν is given, T^* is directly related to the contact time. By using Eq. (26), we can estimate the ratio of the contact time to the mean free time from T^*. For example, $T^*=1\times10^{-4}$ corresponds to $t_r=0.069$ at $\nu=0.1$.

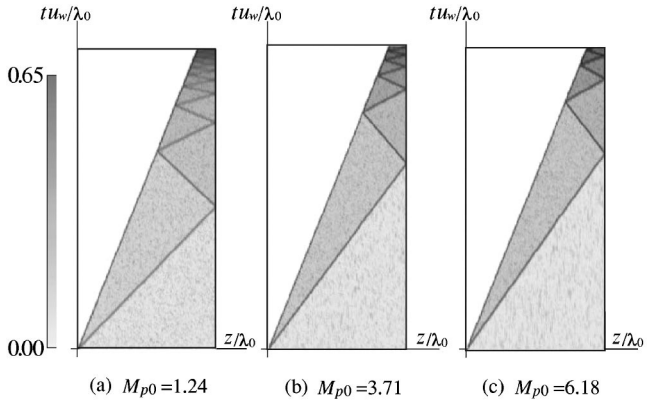

FIG. 4. Propagation of piston-driven shock wave in granular materials (contour of solid fraction ν), $E_p=1\times10^7$ Pa and $\sigma_p=0.30$.

B. Propagation of a piston-shock in granules

In order to examine the properties of the shock wave in soft granular materials, the simulation of the propagation of a piston-driven shock wave in elastic, smooth particles have been performed. As explained above, the initial density, the initial granular temperature, and the piston speed are given as the simulation condition and any boundary condition for statistical variables such as the granular temperature is not applied.

Figure 4 shows the typical results of the DEM simulation for the density profile around a piston-driven shock wave in elastic granular materials. The initial volumetric fraction of particle ν_0 is 0.105. The elastic properties of the particle are indicated in the caption of Fig. 4. The horizontal axis is the dimensionless distance z/λ_0 ($\lambda_0=R/3\sqrt{2}\nu_0$) and the vertical is the dimensionless time tu_w/λ_0. M_{p0} indicates the piston Mach number calculated by the speed of sound in a dilute system and is defined by the initial granular temperature T_0 and the piston speed u_w as

$$M_{p0}=u_w/\sqrt{\gamma T_0}, \tag{27}$$

where γ corresponds to the ratio of specific heats thermodynamically and is 5/3 for monatomic gas. Note that M_{p0} does not indicate the ratio of the piston speed to the speed of sound in a dense system, because the speed of sound is dependent on the solid concentration as explained below. Figure 4 shows that the compression wave is generated in front of the piston and it reflects repeatedly at the piston and the opposite wall with the change in the wave speed. These features are similar to those of the piston-driven shock wave propagating in gas.

Figure 5 shows the numerical results of the density ratio behind and before the shock front ρ_1/ρ_0 ($=\nu_1/\nu_0$), and Fig. 6 shows the ratio of the shock speed to the piston speed U_s/u_w. The simulation for infinite M_{p0} is performed by setting the initial granular temperature $T_0=0$. The solid lines in these figures indicate the results obtained from Rankine-Hugoniot relations for an ideal gas [31]. It is found that, if the system is dilute ($\nu_0=0.0065$), it is close to the molecular gas system and the properties of the shock wave agree with

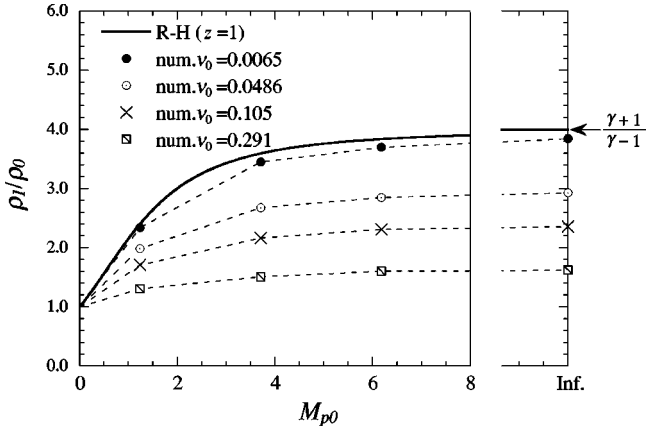

FIG. 5. Relation between the piston Mach number for an ideal gas, M_{p0}, and density ratio ρ_1/ρ_0 for $E_p=1\times10^7$ Pa and $\sigma_p=0.30$.

those of an ideal gas. The density ratio and the shock speed for a strong shock (infinite M_{p0}) can be calculated from Rankine-Hugoniot relations and they are expressed by the ratio of specific heats γ as [31]

$$\frac{\rho_1}{\rho_0}=\frac{\gamma+1}{\gamma-1}, \tag{28}$$

$$\frac{U_s}{u_w}=\frac{\gamma+1}{2}, \tag{29}$$

respectively. Substituting $\gamma=5/3$ into Eqs. (28) and (29), we can obtain $\rho_1/\rho_0=4$ and $U_s/u_w=4/3$ for a dilute limit. The numerical results in a dilute case ($\nu_0=0.0065$) is close to the above values for infinite M_{p0}.

As ν_0 is increased, the shock properties deviate from those of gases. Especially around $\nu_0>0.1$, the shock speed is suddenly increased and it is considerably large in comparison with that of an ideal gas. The dependence of the shock properties on the solid concentration and also the elastic properties of the particle are explained in the following section.

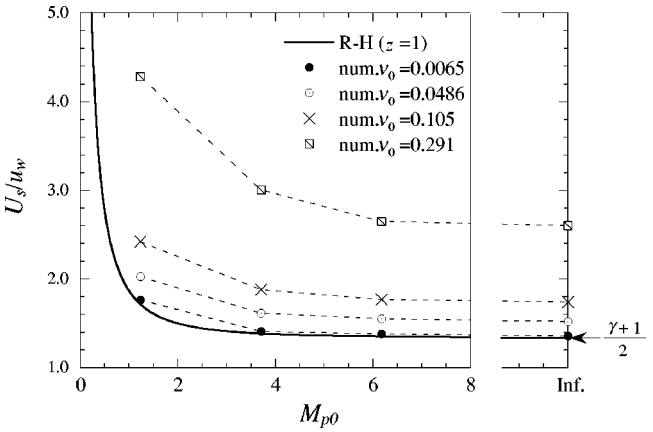

FIG. 6. Relation between the piston Mach number for an ideal gas, M_{p0}, and dimensionless shock speed U_s/u_w for $E_p=1\times10^7$ Pa and $\sigma_p=0.30$.

C. Effect of elasticity on shock properties

By using the equation of state [Eq. (19)] and the equation for internal energy [Eq. (20)], the properties of shock wave propagated in elastic particles can be obtained theoretically. For simplicity, a one-dimensional strong shock wave generated by a piston is considered. Based on the assumption that the pressure and the internal energy before the shock front are much smaller than those behind the shock front, Rankine-Hugoniot conditions for a piston shock wave are given by

$$\rho_0 U_s = \rho_1 (U_s - u_w), \tag{30}$$

$$\rho_0 U_s^2 = p_1 + \rho_1 (U_s - u_w)^2, \tag{31}$$

$$\frac{1}{2} U_s^2 = \frac{1}{2} (U_s - u_w)^2 + \frac{p_1}{\rho_1} + e_1, \tag{32}$$

where u_w indicates the piston speed, U_s is the shock propagation speed, $\rho(=\rho_p \nu)$ is the bulk density, and e is the internal energy per unit mass. The subscripts 0 and 1 indicate the values before and behind the shock front, respectively.

If ρ_0 (or ν_0) and u_w are known, the following relations for ρ_1, p_1, and e_1 are obtained from Eqs. (30)–(32):

$$p_1 - \frac{\rho_0 \rho_1}{\rho_1 - \rho_0} u_w^2 = 0, \tag{33}$$

$$e_1 - \tfrac{1}{2} u_w^2 = 0. \tag{34}$$

On substituting $\rho = \pi \rho_p n^*/6$, the above relations are expressed as functions of n^* and T^*, respectively, and are

$$p(n_1^*, T_1^*) - \frac{\pi}{6} \rho_p u_w^2 \frac{n_0^* n_1^*}{n_1^* - n_0^*} = 0, \tag{35}$$

$$e(n_1^*, T_1^*) - \tfrac{1}{2} u_w^2 = 0. \tag{36}$$

From Eqs. (19) and (20), $p(n^*, T^*)$ and $e(n^*, T^*)$ are given as follows:

$$p(n^*, T^*) = \frac{\pi \rho_p}{6} \left(\frac{\Gamma}{m_p} \right) n^* T^* z(n^*, T^*), \tag{37}$$

$$e(n^*, T^*) = \frac{\Gamma T^*}{m_p} \psi(n^*, T^*). \tag{38}$$

Substituting Eqs. (37) and (38) into Eqs. (35) and (36), the following relations are obtained:

$$n_1^* T_1^* z(n_1^*, T_1^*) - \left(\frac{m_p u_w^2}{\Gamma} \right) \frac{n_0^* n_1^*}{n_1^* - n_0^*} = 0, \tag{39}$$

$$T_1^* \psi(n_1^*, T_1^*) - \frac{1}{2} \left(\frac{m_p u_w^2}{\Gamma} \right) = 0. \tag{40}$$

From the above relations, it is found that the properties of the strong shock wave are characterized by a dimensionless parameter $m_p u_w^2/\Gamma$. In order to obtain n_1^* and T_1^*, the Newton-Raphson method is applied to Eqs. (39) and (40). Let the left-hand sides of Eqs. (39) and (40) equal $f(n_1^*, T_1^*)$ and $g(n_1^*, T_1^*)$, respectively, the following relations are calculated by iteration:

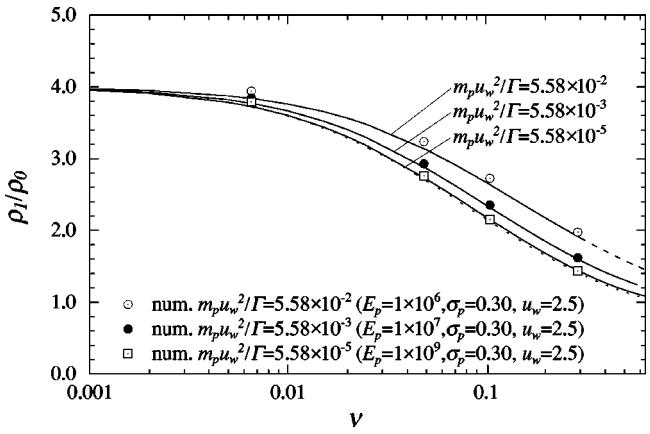

FIG. 7. Relation between the solid fraction before shock front, ν_0, and the density ratio ρ_1/ρ_0 for a strong shock at $T_0 = 0$ (E_p is Young's modulus in Pa, σ_p is Poisson's ratio, and u_w is the piston speed in m/s).

$$\frac{\partial f}{\partial n^*} a^* + \frac{\partial f}{\partial T^*} b^* = -f, \tag{41}$$

$$\frac{\partial g}{\partial n^*} a^* + \frac{\partial g}{\partial T^*} b^* = -g, \tag{42}$$

where $a^* = (n_1^*)_{l+1} - (n_1^*)_l$, $b^* = (T_1^*)_{l+1} - (T_1^*)_l$ and l is the iteration number. The derivatives of f and g are calculated numerically. If the properties of the particle such as m_p and Γ, the piston speed u_w, and the density before the shock $[\rho_0 (= \rho_p \nu_0 = \rho_p \pi n_0^*/6)]$ are given, the properties for the strong shock can be calculated by using n_1^* and T_1^* which are obtained by iteration: density ratio

$$\rho_1/\rho_0 = n_1^*/n_0^*; \tag{43}$$

shock speed

$$U_s = n_1^* u_w/(n_1^* - n_0^*); \tag{44}$$

temperature behind the shock

$$T_1 = \Gamma T_1^*/m_p; \tag{45}$$

and elastic energy behind the shock

$$e_{e1} = \frac{u_w^2}{2} - \frac{3\Gamma T_1^*}{2m_p}. \tag{46}$$

The density ratio ρ_1/ρ_0 and the ratio of the shock speed to the piston U_s/u_w obtained from Eqs. (43) and (44) are shown in Figs. 7 and 8, respectively. In the same way as Figs. 2 and 3, less-accuracy data caused by the approximate

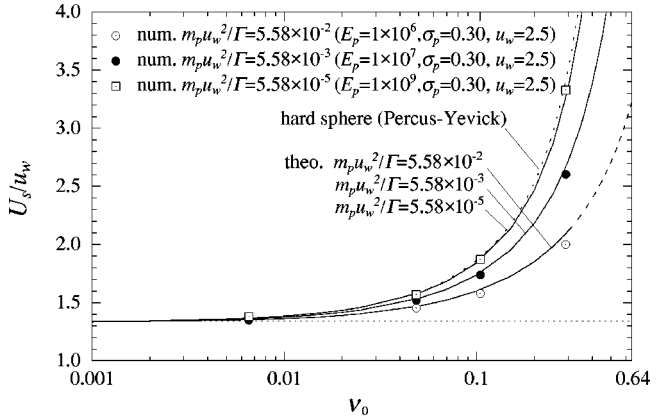

FIG. 8. Relation between the solid fraction before shock front, ν_0, and the dimensionless shock speed U_s/u_w for a strong shock at $T_0=0$ (E_p is Young's modulus in Pa, σ_p is Poisson's ratio, and u_w is the piston speed in m/s).

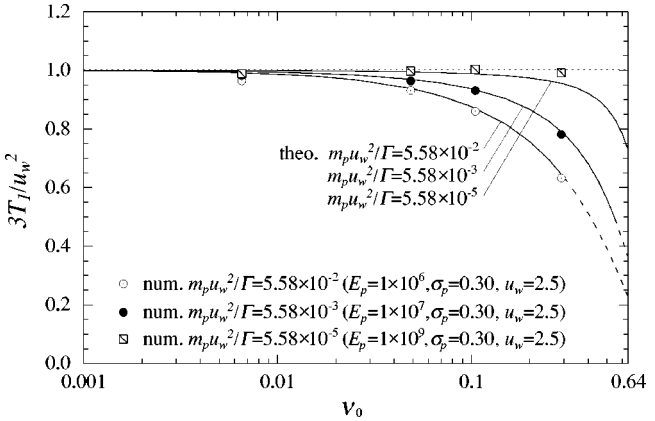

FIG. 9. Relation between the solid fraction before shock front, ν_0, and the dimensionless granular temperature behind shock front $3T_1/u_w^2$ for a strong shock at $T_0=0$ [E_p: Young's modulus (Pa), σ_p: Poisson's ratio and u_w: piston speed (m/s)].

distribution function are shown by the broken lines. Figures 7 and 8 also show the corresponding results obtained from the DEM simulation. They are calculated on the condition that the granular temperature before the shock is $T_0=0$. It is found that the numerical and theoretical results show excellent agreements on various conditions for density and temperature.

If the system is adequately dilute, the effect of the particle collision is insignificant, and in consequence the shock in granular materials behaves as that in ideal gases regardless of the elasticity of the constituent particle. Figures 7 and 8 show that the theoretical results approach to the values for ideal gas, i.e., $\rho_1/\rho_0=4$ and $U_s/u_w=4/3$, respectively, with decreasing ν_0.

In the case of rigid particles, the density ratio and the shock speed are calculated from the compressibility factor derived from the Percus-Yevick equation [Eq. (15)] and Eqs. (30)–(32), and are

$$\frac{\rho_1}{\rho_0}=\frac{3+z_0(\nu_1)}{z_0(\nu_1)}, \tag{47}$$

$$\frac{U_s}{u_w}=\frac{3+z_0(\nu_1)}{3} \tag{48}$$

for the strong shock. As can be seen in Eq. (15), if the system is dilute, the virial term in the equation of state is vanished and z_0 is close to 1. In consequence, Eqs. (47) and (48) approach asymptotically to Eqs. (28) and (29) as z_0 approaches to 1. The solutions of Eqs. (47) and (48) are also plotted in Figs. 7 and 8. In order to obtain these results, the numerical iteration is used since Eq. (47) is an implicit function with respect to ν_1.

From Figs. 7 and 8, it is found that the properties of the shock are close to those of the hard-sphere system if the dimensionless parameter $m_p u_w^2/\Gamma$ is significantly small. As $m_p u_w^2/\Gamma$ is increased, the density behind the shock is increased due to the compressibility of the particles. Consequently, the shock speed is decreased compared with that in the hard-sphere system so as to satisfy the mass conservation given by Eq. (30).

The density ratio and the shock speed in rigid granular materials have been derived from the granular kinetic theory analogous to that of dense gases. Goldshtein *et al.* [12] have defined the radial distribution function $g(\nu)$ for granular materials, which goes to infinity at the maximum packing $\nu=\nu_M$, and have derived the density ratio and the shock speed from the virial equation:

$$\frac{\rho_1}{\rho_0}=\frac{4+4\nu_1 g(\nu_1)}{1+4\nu_1 g(\nu_1)}, \tag{49}$$

$$\frac{U_s}{u_w}=\frac{4+4\nu_1 g(\nu_1)}{3}, \tag{50}$$

where

$$g(\nu)=\frac{1}{1-(\nu/\nu_M)^{4\nu_M/3}}. \tag{51}$$

We compared the solutions by the Percus-Yevick approximation [Eqs. (47) and (48)] with Goldshtein's model [Eqs. (49) and (50)] for $\nu_M=0.64$ (random closest packing) numerically. Both results do not have a significant difference (less than several percent of the absolute value) with regard to the shock properties up to $\nu_0=0.4$.

Figure 9 shows the ratio of the kinetic energy behind the shock $3T_1/2$ to the internal energy $e_1=u_w^2/2$ [see Eq. (34)] obtained from Eq. (45) and the corresponding results by the DEM simulation. It is found that both results are in agreement quantitatively. As mentioned above, the internal energy in elastic particles is divided into the kinetic energy and the elastic energy. If the system is dilute or the particle is sufficiently hard such that the collision between particles occurs instantaneously, most of the internal energy behind the shock turns into the kinetic energy, and the granular temperature T_1 is close to $u_w^2/3$. On the other hand, if the system is dense or

the constituent particle is soft, some of the energy is stored as the elastic deformation. From Fig. 9, it is found that the ratio of the elastic energy to the total energy depends on the parameter $m_p u_w^2/\Gamma$, and is increased as $m_p u_w^2/\Gamma$ is increased.

From these results, it is found that the shock wave propagating in soft granules is influenced by the elastic properties of the constituent particles. As is mentioned above, the energy dissipation due to inelastic collision (including friction) causes a drastic change in the wave propagation. Furthermore, in many actual systems, such as vertically vibrated beds, the force considerably affects the wave propagation and it complicates the matter. The constitutive relations obtained from this analysis are derived on the assumption that the system is idealized (i.e., conservative, in the absence of the gravity), however, they are useful for understanding the dynamic properties of soft particles in various systems.

D. Speed of sound

The speed of sound in a dynamic system of soft granules can be obtained from the equation of state [Eq. (19)] and the equation for the internal energy [Eq. (20)]. The speed of sound a is given from the adiabatic change of the pressure as follows:

$$a = \sqrt{\left(\frac{\partial p}{\partial \rho}\right)_s} = \sqrt{\frac{1}{\rho_p}\left(\frac{\partial p}{\partial \nu}\right)_s}. \tag{52}$$

From the thermodynamic relations, $(\partial p/\partial \nu)_s$ is expressed as follows:

$$\left(\frac{\partial p}{\partial \nu}\right)_s = \left(\frac{\partial p}{\partial \nu}\right)_T + \frac{T}{\rho_p \nu^2}\left(\frac{\partial p}{\partial T}\right)_\nu^2 \left(\frac{\partial e}{\partial T}\right)_\nu^{-1}. \tag{53}$$

Expressing each term of Eq. (53) in z and ψ by using Eqs. (19) and (20), and then substituting into Eq. (52), we obtain the speed of sound in elastic granules as

$$a = \sqrt{zT\left[1 + \frac{q}{z} + \frac{\nu}{z}\left(\frac{\partial z}{\partial \nu}\right)_T\right]}, \tag{54}$$

where

$$q = \frac{[z + T(\partial z/\partial T)_\nu]^2}{\psi + T(\partial \psi/\partial T)_\nu}.$$

If the system is dilute, the compressibility factor $z=1$ and $\psi = 3/2$ because the stored energy due to the elastic deformation is significantly small compared to the kinetic energy. Substituting these values into Eq. (54), the speed of sound for a dilute limit is obtained as

$$a = \sqrt{\frac{5}{3}T}. \tag{55}$$

Equation (55) corresponds to the speed of sound in monatomic gases $\sqrt{\gamma T}$ (the ratio of specific heats $\gamma = 5/3$).

Furthermore, if the particles are rigid, the compressibility factor is only a function of ν as shown in Eq. (15). ψ is equal to 3/2 because the internal energy merely consists of the kinetic energy. Consequently, Eq. (54) becomes *2mm

$$a = \sqrt{z_0 T\left(1 + \frac{2}{3}z_0 + \frac{\nu}{z_0}\frac{dz_0}{d\nu}\right)}. \tag{56}$$

Equation (56) agrees with the speed of sound in the hard-sphere system, which is derived from the kinetic theory of granular materials without energy dissipation [10].

Figure 10 shows the dimensionless speed of sound $a/T^{1/2}$ obtained from Eq. (54). The derivatives of z and ψ in Eq. (54) are calculated numerically in the same way as the method used in the perturbation analysis. From Fig. 10, it is found that the speed of sound decreases with the increase in T^* for a given n^* (or ν). That is, the propagation of an acoustic wave in soft particles is slower than that in hard particles.

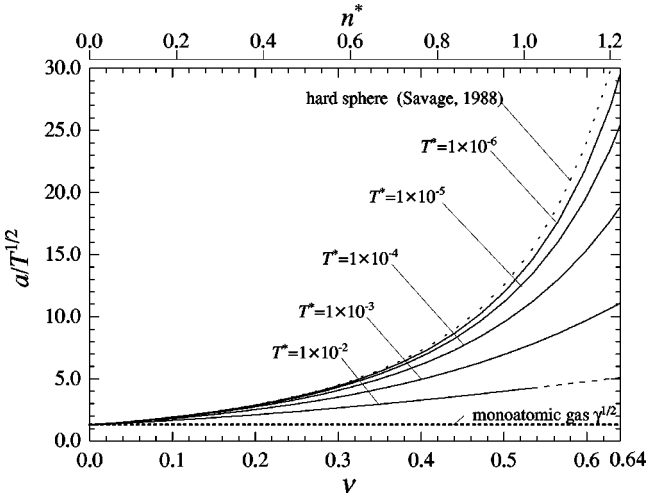

FIG. 10. Speed of sound in elastic granular materials.

V. CONCLUSIONS

Theoretical and numerical studies on wave propagation in a dynamic granular system have been carried out. The thermodynamic perturbation method has been applied to the elastic granular system and some thermodynamicrelations have been derived. The properties of the shock wave in soft particles derived theoretically have been in an excellent agreement with the results of the numerical simulation by the discrete element method. Moreover, the speed of sound has been derived theoretically and compared with the previous study by the kinetic approach. The analyses have quantitatively shown that, from the thermodynamic point of view, the softness of the particle influences the wave not only by a change in the compressibility, but also by a reduction in the temperature due to the conversion to the elastic energy.

ACKNOWLEDGMENTS

This work was begun while S.H. was at the Intelligent Modeling Laboratory, the University of Tokyo. We are grateful to Professor Y. Tsuji and Professor T. Tanaka for making available to us their computer routines. We would like to thank Professor C. E. Brennen for helpful comments on this work. We also thank Professor M. W. Reeks for many variable discussions.

[1] K.M. Aoki and T. Akiyama, Phys. Rev. E **52**, 3288 (1995).
[2] A.V. Potapov and C.S. Campbell, Phys. Rev. Lett. **77**, 4760 (1996).
[3] A. Goldshtein, M. Shapiro, L. Moldavsky, and M. Fichman, J. Fluid Mech. **287**, 349 (1995).
[4] S. McNamara and J.-L. Barrat, Phys. Rev. E **55**, 7767 (1997).
[5] K. Walton, Geophys. J. **92**, 89 (1988).
[6] J.D. Goddard, Proc. R. Soc. London, Ser. A **430**, 105 (1990).
[7] C–h. Liu and S.R. Nagel, Phys. Rev. Lett. **68**, 2301 (1992).
[8] S. Melin, Phys. Rev. E **49**, 2353 (1994).
[9] E. Hascoët, H.J. Herrmann, and V. Loreto, Phys. Rev. E **59**, 3202 (1999).
[10] S.B. Savage, J. Fluid Mech. **194**, 457 (1988).
[11] A. Goldshtein and M. Shapiro, J. Fluid Mech. **282**, 75 (1995).
[12] A. Goldshtein, M. Shapiro, and C. Gutfinger, J. Fluid Mech. **316**, 29 (1996).
[13] V. Kamenetsky, A. Goldshtein, M. Shapiro, and D. Degani, Phys. Fluids **12**, 3036 (2000).
[14] W.G. Hoover and F.H. Ree, J. Chem. Phys. **49**, 3609 (1968).
[15] V.I. Kalikmanov, *Statistical Physics of Fluids* (Springer, New York, 2001).
[16] P.A. Cundall and O.D.L. Strack, Geotechnique **29**, 47 (1979).
[17] Y.–h. Taguchi, Phys. Rev. Lett. **31**, 1367 (1992).
[18] Y. Tsuji, T. Tanaka, and T. Ishida, Powder Technol. **71**, 239 (1992).
[19] S.P. Timoshenko and J.N. Goodier, *Theory of Elasticity* (McGraw–Hill, New York, 1982).
[20] M. Woo and I. Greber, AIAA J. **37**, 215 (1999).
[21] R.W. Zwanzig, J. Chem. Phys. **22**, 1420 (1954).
[22] J.A. Barker and D. Henderson, J. Chem. Phys. **47**, 2856 (1967).
[23] G.A. Mansoori and F.B. Canfield, J. Chem. Phys. **51**, 4958 (1969).
[24] W.G. Hoover, *Computational Statistical Mechanics* (Elsevier, Amsterdam, 1991).
[25] J.K. Percus and G.J. Yevick, Phys. Rev. **110**, 1 (1958).
[26] M.S. Wertheim, Phys. Rev. Lett. **10**, 321 (1963).
[27] E. Thiele, J. Chem. Phys. **39**, 474 (1963).
[28] G.A. Mansoori, J.A. Provine, and F.B. Canfield, J. Chem. Phys. **51**, 5295 (1969).
[29] G.J. Throop and R.J. Bearman, J. Chem. Phys. **42**, 2408 (1965).
[30] J.P. Hansen and I.R. McDonald, *Theory of Simple Liquids* (Academic, New York, 1986).
[31] J.D. Anderson, *Modern Compressible Flow* (McGraw-Hill, New York, 1982).